Free surface entropic lattice Boltzmann simulations of film condensation on vertical hydrophilic plates

Hygum, Morten Arnfeldt; Karlin, Iliya; Popok, Vladimir

Published in:
International Journal of Heat and Mass Transfer

DOI (link to publication from Publisher):
10.1016/j.ijheatmasstransfer.2015.04.032

Publication date:
2015

Document Version
Early version, also known as pre-print

International Journal of Heat and Mass Transfer 87 (2015) 576–582

Contents lists available at ScienceDirect

International Journal of Heat and Mass Transfer

journal homepage: www.elsevier.com/locate/ijhmt

Free surface entropic lattice Boltzmann simulations of film condensation on vertical hydrophilic plates

Morten A. Hygum [a,*], Iliya V. Karlin [b], Vladimir N. Popok [a]

[a] Department of Physics and Nanotechnology, Aalborg University, 9220 Aalborg, Denmark
[b] Department of Mechanical and Process Engineering, ETH Zurich, 8092 Zurich, Switzerland

ARTICLE INFO

Article history:
Received 9 January 2015
Received in revised form 31 March 2015
Accepted 11 April 2015

Keywords:
Film condensation
Entropic lattice Boltzmann
Free surface lattice Boltzmann

ABSTRACT

A model for vapor condensation on vertical hydrophilic surfaces is developed using the entropic lattice Boltzmann method extended with a free surface formulation of the evaporation–condensation problem. The model is validated with the steady liquid film formation on a flat vertical wall. It is shown that the model is in a good agreement with the classical Nusselt equations for the laminar flow regime. Comparisons of the present model with other empirical models also demonstrate good agreement beyond the laminar regime. This allows the film condensation modeling at high film Reynolds numbers without fitting, tuning or empirical parameters.

1. Introduction

Condensation processes play a crucial role in various engineering and scientific aspects affecting energy conversion, safety and reliability issues as well as design aspects of devices and constructions. Condensation can be divided into two main types: dropwise and film condensation [1,2]. Dropwise condensation occurs on hydrophobic surfaces. Alternatively, condensate can wet the surface and form a film. This case is typical for hydrophilic surfaces. Since the thermal resistance is low at dropwise condensation the heat transfer is significantly higher than for the film condensation. Moreover, in order to consider droplet formation, a number of parameters need to be taken into account and modeling becomes rather involved. Therefore, a majority of the models are developed for the film condensation.

The first model for film condensation was introduced almost a century ago by Nusselt [3]. Nevertheless, Nusselt's model remains very popular and it is often used because in this case the closed-form analytical solution is available. Nusselt's model assumes (i) a linear temperature distribution across the film condensate, (ii) constant film properties, (iii) the shear stress at the surface and inertia effects are negligible, (iv) laminar flow in the forming film, and (v) pure still vapor from which the condensation occurs. In Fig. 1 an illustration of the system considered by Nusselt is shown. Nusselt obtained analytical expressions for the velocity profile in the film, the film thickness, mass flow and the heat transfer coefficient along a hydrophilic wall.

Nusselt's model has been found to have a good accuracy but only for low flow velocities [2]. One of the reasons for low accuracy at high flow velocities is the neglect of inertia and interface shear effects. The role of these effects has been intensely studied in the literature and it has been found that at low Prandtl numbers the interface shear must be taken into account while at high Prandtl numbers the effect of shear is small and can be neglected [4,5]. Both effects (inertia and interface shear) lower the mass flow rate. Also, subcooling effects are discarded in Nusselt's model which may alter the condensation flux at the liquid–gas interface. In [2] it is shown how the above effects can be taken into account.

Nusselt's model also assumes a laminar film without ripples or waves at the interface. This assumption has been studied and found to be valid for film Reynolds numbers $Re_f \lesssim 33$ [6]. To classify different condensation flows the film Reynolds number is defined as

$$Re_f = \frac{4\dot{m}(z=L)}{\mu_l}, \tag{1}$$

where $\dot{m}$ is the mass flow in the bottom of the film at the length L and μ_l is the dynamic viscosity of the film. For $Re_f \gtrsim 33$ the condensate film turns wavy-laminar and for $1000 \lesssim Re_f \lesssim 1800$ the flow in the film becomes turbulent [2]. These surface wave and turbulence effects have been suggested to alter the film thickness that leads to a significant change in the heat transfer coefficient. Therefore, it is normal practice to use empirical correlations for these regimes [1,2].

On the other hand, the lattice Boltzmann (LB) method has over the last two decades become a successful numerical approach to

* Corresponding author.

http://dx.doi.org/10.1016/j.ijheatmasstransfer.2015.04.032
0017-9310/

efficiently simulate various complex flows [7–14]. Different LB methods for multiphase flows have been suggested [15] and recently a LB model to predict film and dropwise condensation was developed [16,17] using the so-called Shan-Chen multiphase method. It was, however, reported that the model becomes numerically unstable if the Prandtl number deviates from one. Furthermore, a general issue using the Shan-Chen method is that the interface between the vapor and the liquid is diffuse [15].

To address tracking of interfaces between the gas and liquid phases as well as further strengthen the model, a free surface LB (FSLB) methods have been developed [18–20]. However, to ensure numerical stability, adaptive time steps [19] or adaptive grids [21] need to be implemented in the model which causes a significant complication.

In this paper we suggest a free surface entropic LB (FSELB) model and demonstrate how the model can be used to predict film condensation. Unlike the previous LB models, the entropic LB scheme in the free-surface framework demonstrates excellent stability and accuracy without considering adaptive grid or time steps. Furthermore, the model is not limited to laminar flows and, thus, it is applicable to laminar, wavy-laminar and turbulent film flows. We consider the construction in detail in two dimensions (2D); extension to 3D is straightforward.

It is worth mentioning that a lattice Boltzmann condensation model with no limitation on model parameters has not been developed so far. Moreover, the presented model is the first FSELB model. Finally, adding mass transfer to the liquid–vapor interface in FSLB methods is an extension which to our best knowledge have not been reported before. Thus, FSELB allows for modeling of more complex processes, e.g. evaporation and condensation.

The outline of the paper is as follows: in Section 2.1 the entropic lattice Boltzmann (ELB) model will be described and in Section 2.2 the modeling of the temperature field is presented. In Section 2.3 the FSLB method developed in [19] is reviewed and in order to validate the FSELB model the key concepts and equations of Nusselt's model are presented in Section 2.4. Finally, in Section 2.5 the set-up of our model will be described showing how it is developed from the FSLB framework. The results are presented and discussed in Section 3 while Section 4 concludes the paper.

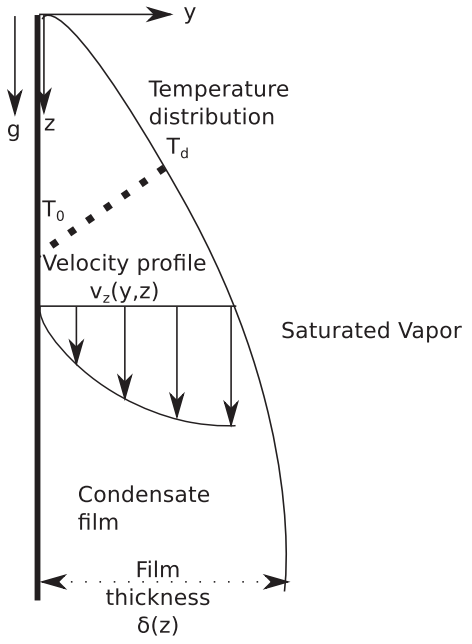

Fig. 1. Film condensation on a vertical surface according to Nusselt's model. T_o is the wall temperature and T_d is the temperature at the interface between the gas and liquid phase.

2. Model descriptions

The 2D FSELB model, presented here, is constructed using the ELB approach for modeling of the flow in the film. The liquid–gas interface is treated as a boundary according to the FSLB framework and the temperature field is treated as a passive scalar described below in Section 2.2.

2.1. Entropic lattice Boltzmann

The LB method concerns a discrete kinetic equation which solves for populations $f_i(\vec{x},t)$ corresponding to discrete velocities $\vec{c}_i, i = 1,..,n_d$. The velocities fit into a regular spatial lattice with the nodes $\vec{x}$. The ELB method is a generalization of the LB method and involves restoring the second law of thermodynamics. This additional step renders excellent non-linearly numerical stability and drastically reduces the computational demand at high Reynold numbers [11,22].

The ELB equation with the lattice Bhatnagar–Gross–Krook (LBGK) collision operator including a body force is given as [11]

$$f_i(\vec{x}+\vec{c}_i dt, t+dt) = f_i(\vec{x},t) + \alpha\beta(f_i^{eq}(\rho,\vec{u}) - f_i(\vec{x},t)) + f_i^{eq}(\rho,\vec{u}+\Delta\vec{u}) - f_i^{eq}(\rho,\vec{u}), \quad (2)$$

where β is related to the kinematic viscosity v as follows:

$$v = c_s^2\left(\frac{1}{2\beta} - \frac{1}{2}\right)dt. \quad (3)$$

Here, c_s is the speed of sound in the model, dt is the time step, ρ is the density, $\vec{u}$ is flow velocity, and α is the non-trivial root of the entropy estimate which will be described below. The density and momentum are obtained from the populations as:

$$\rho = \sum_{i=1}^{n_d} f_i \quad (4)$$

and

$$\rho\vec{u} = \sum_{i=1}^{n_d} \vec{c}_i f_i. \quad (5)$$

The body force is incorporated using the exact difference method which provides the expression for the velocity increment $\Delta\vec{u}$ as [23]

$$\Delta\vec{u} = \frac{\vec{F}}{\rho}dt, \quad (6)$$

where the force $\vec{F} = \vec{g}\rho$ with $\vec{g}$ to be the gravitational acceleration. The actual fluid velocity $\vec{U}$ is obtained by averaging the fluid momentum before and after the collision:

$$\rho\vec{U} = \rho\vec{u} + \frac{dt\vec{F}}{2}. \quad (7)$$

The equilibrium function f_i^{eq} is the minimizer of the discrete entropy function H under local conservation laws of mass and momentum. The entropy function is given as

$$H = \sum_{i=1}^{n_d} f_i \ln\frac{f_i}{W_i}, \quad (8)$$

with W_i to be the lattice specific weights. Expanding the minimization problem to the order u^2 gives rise to

$$f_i^{eq}(\rho,\vec{u}) = \rho W_i\left(1 + \frac{\vec{c}_i\cdot\vec{u}}{c_s^2} + \frac{(\vec{c}_i\cdot\vec{u})^2}{2c_s^4} - \frac{\vec{u}\cdot\vec{u}}{2c_s^2}\right). \quad (9)$$

The entropy balance is maintained at each node for each time step through the parameter α. It is obtained as the non-trivial root of the following equation:

$$H(f) = H(f + \alpha(f^{eq} - f)). \tag{10}$$

In order to ensure an efficient simulation the following asymptotic expansion for α is used for the condition $|(f_i^{eq} - f_i)/f_i| < 10^{-2}$ [24]:

$$\alpha = 2 - \frac{4a_2}{a_1} + \frac{16a_2^2}{a_1^2} - \frac{8a_3}{a_1} + \frac{80a_3a_2}{a_1^2} - \frac{80a_2^3}{a_1^3} - \frac{16a_4}{a_1}, \tag{11}$$

with the coefficients a_n obtained from

$$a_n = \frac{(-1)^{n-1}}{n(n+1)} \sum_{i=1}^{n_d} \frac{(f_i^{eq} - f_i)^{n+1}}{f_i^n}, \qquad n \geqslant 1. \tag{12}$$

If $|(f_i^{eq} - f_i)/f_i| > 10^{-2}$ then α is found using the bi-section method.

The D2Q9 lattice [8] is chosen for the model. For that lattice

$$\begin{aligned} c_x &= (0, 1, 0, -1, 0, 1, -1, -1, 1), \\ c_y &= (0, 0, 1, 0, -1, 1, 1, -1, -1), \\ W &= (4/9, 1/9, 1/9, 1/9, 1/9, 1/36, 1/36, 1/36, 1/36), \end{aligned} \tag{13}$$

and $c_s = 1/\sqrt{3}$.

ELBM was originally developed to stabilize simulations of high Reynolds number, with large velocity gradients. The film flows, considered here, are not such systems. However, ELBM can still be adapted to ensure better stability of free surface simulations. As shown later, in Section 3, the source of numerical instability for the free surface simulations carried out in this paper is found to be the surface itself. Utilizing the ELBM approach, thus, allows for better stability for a wider range of input parameters.

2.2. Temperature field

One of the simplest LB realizations for modeling the temperature T is to treat it as a passive scalar. As suggested in [25] the temperature field can, thus, be solved using a second lattice. Here, the D2Q9 lattice is also considered. More advanced models do exist which e.g. include viscous heating [26]. However, while neglecting these effects the kinetic equation for the second population, representing T, is given as [25]

$$g_i(\vec{x} + \vec{c}_i dt, t + dt) = g_i(\vec{x}, t) + 2\beta_T(g_i^{eq}(T, \vec{u}) - g_i(\vec{x}, t)), \tag{14}$$

where the thermal diffusivity

$$D_T = c_s^2\left(\frac{1}{2\beta_T} - \frac{1}{2}\right)dt. \tag{15}$$

The temperature is obtained from $T = \sum_{i=1}^{n_d} g_i$ and the equilibrium function g_i^{eq} is

$$g_i^{eq}(T, \vec{u}) = TW_i\left(1 + \frac{\vec{c}_i \cdot \vec{u}}{c_s^2}\right). \tag{16}$$

Eq. (14) is acceptable for the use in our model. As mentioned, the source of numerical instability does not originate from the temperature field which is why the LBGK relaxation is sufficient.

2.3. Free surface modeling

The free surface modeling is based on the approach described in [19] and for the sake of completeness the key points are presented here.

In the free surface model the gas phase is assumed to have a negligible effect on the fluid flow in the film. Therefore, surface tension and shear stress at the liquid–vapor interface are discarded. Moreover, the contact angle at the top of the film is found to have a negligible effect when considering film condensation [16] which justifies the simplification. As in any numerical realization the domain is discretized with a suitable set of nodes. Every node has one of the following flags: fluid/filled node, interface node, or an gas/empty node, where the complication lies within the treatment of the interface nodes. An overview of the surface handling is shown in Fig. 2.

2.3.1. Interface movement

The movement of the interface is modeled by keeping track of the mass m and the fluid fraction ϵ in each node. The fluid fraction $\epsilon = m/\rho$ is one ($\epsilon = 1$) for a filled node, zero for an empty node ($\epsilon = 0$), and $0 < \epsilon < 1$ for an interface node. Mass fluxes between the nodes are directly computed through the streaming step, which for an interface node at $\vec{x}$ and a fluid node at $\vec{x} + \vec{c}_i$ becomes

$$\Delta m_i^F(\vec{x}, t + dt) = f_{\tilde{i}}(\vec{x} + \vec{c}_i, t) - f_i(\vec{x} + \vec{c}_i, t), \tag{17}$$

where $\tilde{i}$ is the opposite direction of $i : \vec{c}_{\tilde{i}} = -\vec{c}_i$. The notation ^{F} denotes that the neighbor is a fluid node.

The mass exchange between two interface nodes must account for the area between the nodes. This is approximated by the average of the fluid fractions of the two nodes as follows:

$$\Delta m_i^I(\vec{x}, t + dt) = \left[f_{\tilde{i}}(\vec{x} + \vec{c}_i, t) - f_i(\vec{x} + \vec{c}_i, t)\right] \frac{\epsilon(\vec{x} + \vec{c}_i, t) + \epsilon(\vec{x}, t)}{2}, \tag{18}$$

where ^{I} denotes that the neighbor is an interface node. Thus, the mass of the interface node at $\vec{x}$ at the next time step is given as

$$m(\vec{x}, t + dt) = m(\vec{x}, t) + \sum_{i=1}^{n_d} \Delta m_i^k(\vec{x}, t + dt), \tag{19}$$

with $k = \{F, I\}$.

2.3.2. Surface reconstruction

At the interface nodes the populations which would have streamed from the empty nodes are lacking and must therefore be reconstructed. It is assumed that the pressure at the interface gives rise to a density $\rho_A = 1$ and that the vapor does not affect the film flow. This allows for

$$f_i'(\vec{x}, t + dt) = f_i^{eq}(\rho_A, \vec{u}) + f_{\tilde{i}}^{eq}(\rho_A, \vec{u}) - f_i(\vec{x}, t), \tag{20}$$

with f_i' to be the post-streaming populations. Note that the surface tension can be included by modifying Eq. (20), see [27,28]. Using Eq. (20) we get a full set of populations. However, in order to balance

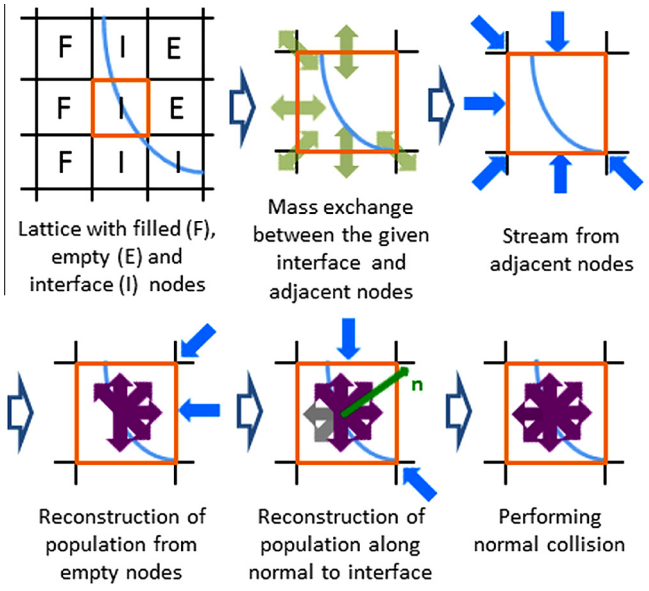

Fig. 2. Overview of the steps that have to be executed for the interface handling.

the force at each side of the interface, Eq. (20) is used for streaming along the direction of the normal vector $\vec{n}$ to the surface. Thus, if

$$\vec{n}\cdot\vec{c}_i > 0, \qquad \vec{n} = \frac{1}{2}\begin{pmatrix} \epsilon(\vec{x}_{j-1,k}) + \epsilon(\vec{x}_{j+1,k}) \\ \epsilon(\vec{x}_{j,k-1}) + \epsilon(\vec{x}_{j,k+1}) \end{pmatrix}, \tag{21}$$

with j being the x-coordinate and k being the y-coordinate, Eq. (20) is also used for the streaming.

2.3.3. Surface re-initialization

After the density and the momentum have been calculated it must be investigated whether the interface nodes have been filled or emptied during the time step. This is done according to:

$$\begin{aligned} m(\vec{x}, t+dt) &> (1+\kappa)\rho(\vec{x}, t+dt) \quad \rightarrow \text{node filled} \\ m(\vec{x}, t+dt) &< -\kappa\rho(\vec{x}, t+dt) \quad \rightarrow \text{node emptied} \end{aligned} \tag{22}$$

where $\kappa = 10^{-4}$ is a threshold to prevent a re-initialization of the given node at the next time step. For implementation reasons the coordinate of the node of interest is stored in a separate list and the conversion is done when the main loop is executed for all nodes.

An empty node must have a mass equal to zero and a filled node must have a mass equal to the density times the volume. As in standard LB units we set $dx = dy = 1$ and $\rho = 1$. Therefore, the use of Eq. (22) inevitably leads to an excess mass m^{ex} which must be distributed to the neighboring interface nodes. The excess mass is given as following:

$$\begin{aligned} m^{ex} &= m \qquad\quad \rightarrow \text{ emptied node} \\ m^{ex} &= m - \rho dxdy \;\rightarrow \text{ filled node.} \end{aligned} \tag{23}$$

It can be noticed, that if the emptied node has a numerically negative mass, the interface has moved beyond the current node. Similarly, if the mass of a filled node gives rise to a density larger than one the interface has moved past the node.

The conversion of the newly filled or emptied node must first be done. For a newly filled node the surrounding empty nodes are converted to interface nodes. For each of these nodes the average density ρ^{avg} and momentum $\rho^{avg}\vec{u}^{avg}$ are calculated considering the neighboring fluid and interface nodes. The newly converted interface nodes are then initialized with equilibrium functions $f_i^{eq}(\rho^{avg}, \vec{u}^{avg})$. Similarly, the fluid neighbors to the newly emptied nodes are converted to interface nodes. The former nodes population is used for each corresponding new interface node.

The last step is to distribute the excess mass to the neighboring interface nodes. The excess mass is weighted according to $\vec{n}$. Thus, the distribution of excess mass is calculated according to

$$m(\vec{c}+\vec{c}_i) = m(\vec{c}+\vec{c}_i) + m^{ex}\frac{\eta_i}{\eta_{total}}, \tag{24}$$

with η_{total} to be the sum of all the weights η_i, which are obtained according to

$$\begin{aligned} \eta_i &= \begin{cases} \vec{n}\cdot\vec{c}_i & \text{if } \vec{n}\cdot\vec{c}_i > 0 \\ 0 & \text{otherwise} \end{cases} \quad \text{filled nodes} \\ \eta_i &= \begin{cases} -\vec{n}\cdot\vec{c}_i & \text{if } \vec{n}\cdot\vec{c}_i < 0 \\ 0 & \text{otherwise} \end{cases} \quad \text{emptied nodes.} \end{aligned} \tag{25}$$

With the excess mass distributed, the re-initialization is completed and the simulation can continue to the next time step. It can, however, happen that single interface nodes are left behind the flow or interface nodes get trapped inside the fluid. These are artifacts but they do not perturb the flow. In order to remove these artifacts the procedure described in [19] is applied.

2.4. The Nusselt model

With the LB framework of the model described we proceed with its validation. For that we need to introduce a few key equation of the Nusselt model described in [2] and refer once again to the condensation process illustrated in Fig. 1. The Nusselt formulas can be derived by considering the Navier–Stokes equation at steady-state combined with the enthalpy balance. The flow is due to gravity and the film thickness arises from the condensing mass flux at the liquid–vapor interface. The film thickness is obtained as

$$\delta(z) = \left[\frac{4k_l\mu_l(T_d - T_0)z}{\Delta h_{vap}\rho_l(\rho_l - \rho_g)g}\right]^{1/4}, \tag{26}$$

with k_l to be the thermal conductivity of the liquid, T_0 to be the wall temperature, T_d to be the temperature at the interface between the gas and liquid phases, Δh_{vap} to be the latent heat of condensation, ρ_l to be the density of the liquid, ρ_g to be the density of the gas, and g to be the acceleration due to gravity. The velocity profile v is given as

$$v = \frac{(\rho_l - \rho_g)g}{\mu_l}\left[y\delta - \frac{y^2}{2}\right] \tag{27}$$

and the mass flow rate $\dot{m}$ is, according to Nusselt, given as

$$\dot{m} = \rho_l\frac{(\rho_l - \rho_g)g}{3\mu_l}\delta^3. \tag{28}$$

The local heat transfer coefficient h is given as $h = k_l/\delta$ which leads to the average heat transfer coefficient as follows:

$$\bar{h} = \frac{4}{3}\frac{1}{4^{1/4}}\left[\frac{k_l^3\Delta h_{vap}\rho_l(\rho_l - \rho_g)g}{\mu_l(T_d - T_0)L}\right]^{1/4} \approx 0.943\left[\frac{k_l^3\Delta h_{vap}\rho_l(\rho_l - \rho_g)g}{\mu_l(T_d - T_0)L}\right]^{1/4}, \tag{29}$$

where L is the length of the film. This allows for the non-dimensional Nusselt formula of the averaged heat flux:

$$H_f = \frac{\bar{h}}{k_l}\left[\frac{\mu_l^2}{\rho_l(\rho_l - \rho_g)g}\right]^{1/3} = 1.47Re_f^{-1/3}. \tag{30}$$

With the theoretical foundation in place the set-up of our model will be presented below. The model is developed in the way that it can be compared with the Nusselt formulas as a benchmark.

2.5. Simulation set-up

Similar to the Nusselt formulation the surface tension is considered to be negligible and the pressure of the vapor is assumed to be constant and saturated in our model.

A computation domain of $N_x \times N_y = 300 \times 300$ is proven to yield grid independent results. At the wall boundary the no-slip condition and the temperature T_0 are applied. The no-slip condition is realized with the bounce-back method. The temperature at the interface is set to T_0using the approach presented in [29] and at the bottom the extrapolation boundaries is applied according to the procedure suggested in the same reference. The top nodes are fixed as vapor nodes and therefore never addressed. At the interface the temperature T_d is enforced.

The condensation flux couples the energy equation to the mass flux at the interface. The energy conservation at the surface implies

$$k_l\vec{\nabla}T|_{interface} = k_g\vec{\nabla}T|_{interface} - \vec{J}\Delta h_{vap}, \tag{31}$$

with $\vec{J}$ to be the condensation flux and k_g to be the thermal conductivity of the gas.

The contribution of the condensation flux is added to the right side of Eq. (19) for the mass at the interface, thus, converting it to

$$m(\vec{x}, t+dt) = m(\vec{x}, t) + \sum_{i=1}^{n_d} \Delta m_i^k(\vec{x}, t+dt) + AJdt, \tag{32}$$

with A to be the area of the surface at the given node. This area, which for 2D simulations correspond to a line, is found by assuming that the area of the interface can be approximated by a right-angled triangle. Note, that this additional mass flux is our extension to the FSLB framework to be able to address condensation-evaporation problems.

The fluid flow and heat transfer of steady film condensation on hydrophilic surfaces can be characterized by the following two dimensionless numbers:

$$Pr = \frac{\nu}{D_T} = \frac{c_p \mu_l}{k_l}, \qquad Ja = \frac{c_p(T_d - T_0)}{\Delta h_{\text{vap}}}, \tag{33}$$

which are the Prandtl and Jakob numbers, respectively, and c_p is the specific heat at constant pressure. The Prandtl number is a material constant and the Jakob number is the ratio of the sensible heat of the film and the latent heat of the vapor. Thus, for a fixed Pr the film thickness will increase with the Jakob number since the energy flux at the interface increases.

3. Results and discussion

3.1. Comparisons of FSELB with the Nusselt model

In Fig. 3 film thickness modeled by the developed FSELB method and the classic Nusselt model are compared for two pairs of Prandtl and Jakob numbers, $Pr = 7$ and $Ja = 0.185$, and $Pr = 0.8$ and Ja = 0.4. These parameters were chosen, in order to demonstrate that the model works well within some range of input parameters. For all the simulations $L = 1$ mm, $g = 9.81$ m/s, $\rho = 10^3$ kg/m^3, $\Delta H_{vap} = 2260$ kJ/kg, $\mu_l = 1.002 \cdot 10^{-3}$ Pa · s. k_l and $(T_d - T_0)$ is calculated from Pr and Ja, respectively. As in normal LB practice, the velocity is set so that it does not exceed 0.05 in lattice units. It is seen that our simulations agree well with those carried out using the analytical Nusselt formula.

Comparisons of z-components of the velocities between the two models are shown in Fig. 4 along with the film Reynolds numbers. The mass flow in the FSELB model is calculated by the following formula:

$$\dot{m} = \sum_{y=1}^{y_f} u_y \rho_y dy, \tag{34}$$

where y_f is the y-coordinate of the interface node at L. It can be seen that both models agree well for low length values. However, the velocities predicted by the FSELB model are found to be smaller than those calculated by Nusselt model's and this difference increases with the velocity rise. Actually, this is expected behavior because the FSELB method takes into consideration the effects of inertia forces which lowers the velocity.

The same tendencies were found in [4,16] where the deviation was found to be the highest for high Jakob numbers and low Prandtl numbers. According to [4,16] inertia, shearing stress and viscous effects become increasingly important at high Jakob numbers and low Prandtl numbers which is where the present FSELB model also deviates from the Nusselt model.

The dimensionless temperature $\theta = \frac{T - T_0}{T_0 - T_d}$ profile at L and mean heat transfer coefficient for the two models are compared in Fig. 5. It is seen that the linear approximation of the temperature is a quite suitable approach for predicting the mean heat transfer coefficient in the laminar regime.

In Fig. 6 the contours of T and v are shown for simulations with $Pr = 7$ and $Ja = 0.185$. The contours of T and v for simulations with $Pr = 0.8$ and $Ja = 0.4$ are presented in Fig. 7. Good agreement between the profiles modeled with FSELB and the Nusselt formulas can be seen.

3.2. Beyond the laminar regime

As mentioned in the introduction, the Nusselt model has experimentally been proven to be true only for $Re_f < 30$. Beyond this regime empirical expressions were developed. In this paper we use two expressions proposed by Kutateladze [30] and Chen et.

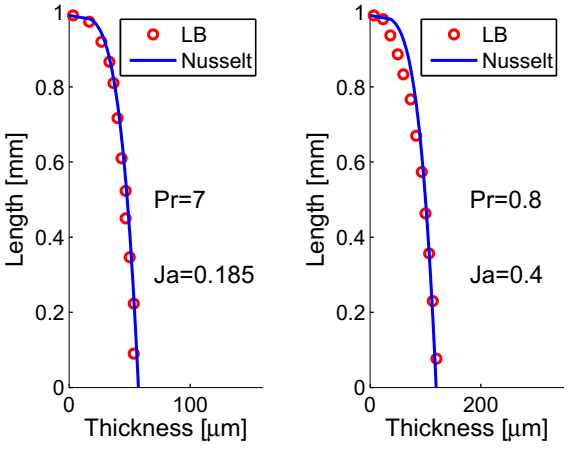

Fig. 3. Comparisons of film thicknesses predicted by FSELB simulation and Nusselt formula.

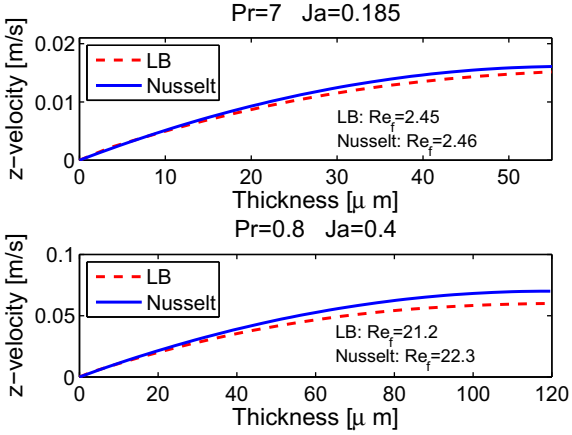

Fig. 4. Comparisons of z-components of the velocities predicted by FSELB simulation and Nusselt formula.

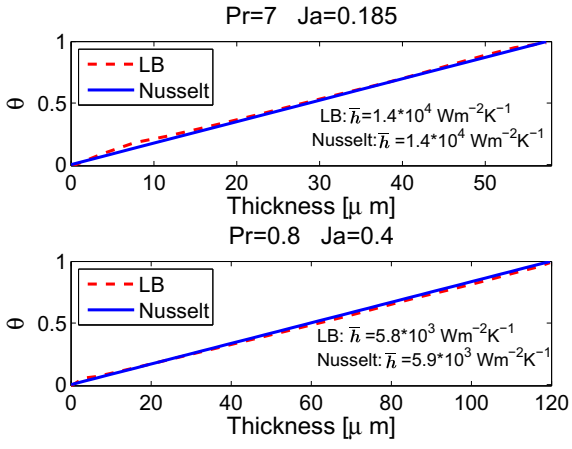

Fig. 5. Comparisons of dimensionless temperature profiles predicted by FSELB simulation and Nusselt formula.

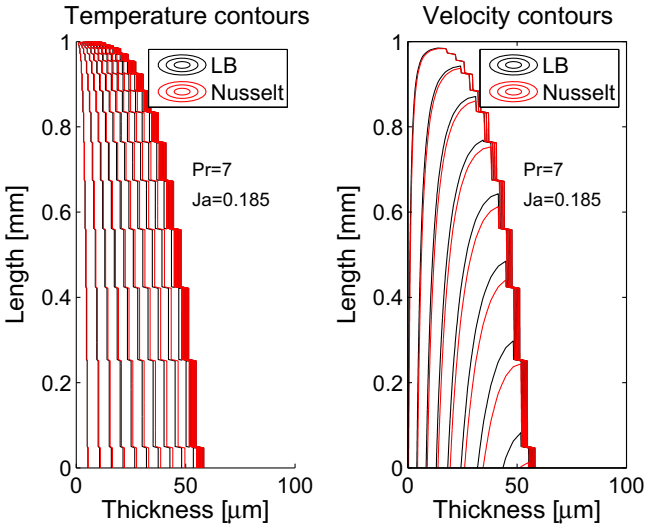

Fig. 6. Comparisons of temperature and velocity contour profiles predicted by FSELB simulation and Nusselt formula with $Pr = 7$ and $Ja = 0.185$.

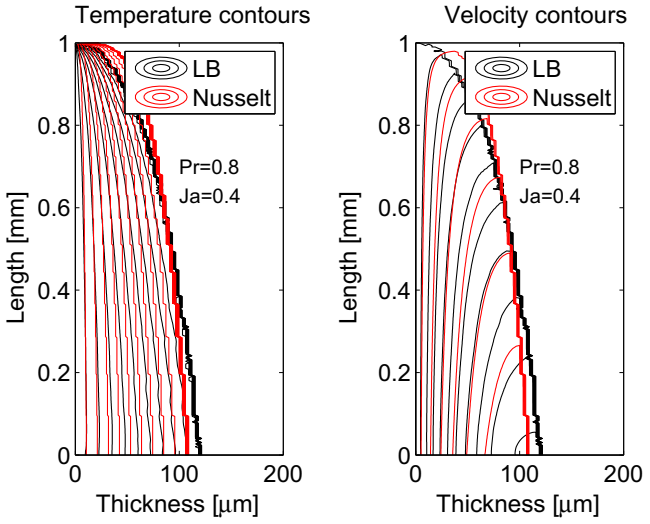

Fig. 7. Comparisons of temperature and velocity contour profiles predicted by FSELB simulation and Nusselt formula with $Pr = 0.8$ and $Ja = 0.4$.

al [31] for comparisons with our model. Since the presented model is in 2D, only comparisons for the wavy-laminar regime is carried out.

In Fig. 8 the non-dimensional averaged heat flux is compared to the Nusselt formula and the empirical models proposed by Kutateladze [30] and Chen et. al [31]. It can be seen, that the simulations using FSELB model show a reasonable agreement with the two empirical models for the range of used film Reynolds numbers while the Nusselt calculations significantly underestimate the flux especially for high Reynolds numbers.

It is worth mentioning that wave-like behavior of the film can be simulated by the presented FSELB approach with high enough resolution. To illustrate this, two simulations were conducted with same input parameters and initial conditions but with different resolutions, namely 600×600 and 3000×3000 grids. The simulations are carried out with $Pr = 0.5, Ja = 2.5$ and $L = 200$ mm. A snapshot of both simulations where $Re_f = 94.65$ can be found in Fig. 9. It is seen that the film becomes wave-like when simulated with high resolution. This indicates that the present approach can be used beyond the laminar flow regime. A detailed study of

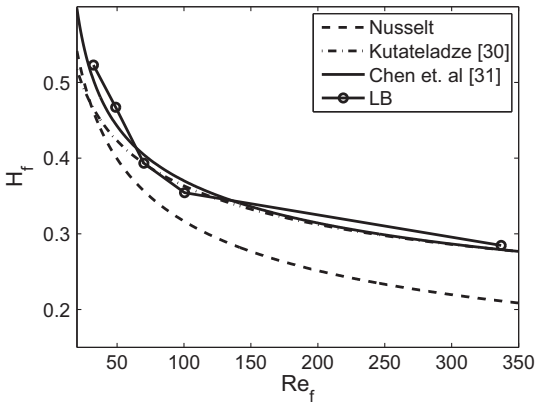

Fig. 8. Comparison of non-dimensional averaged heat fluxes predicted by the various models for the given range of film Reynolds numbers.

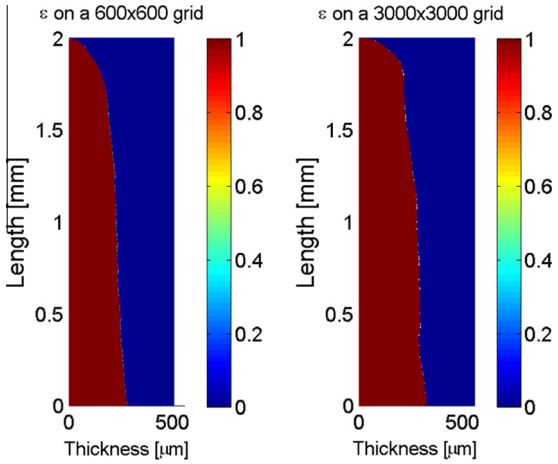

Fig. 9. Comparison of fluid fraction ϵ profiles at a snapshot where $Re_f = 94.65$. The simulations are carried out with two different resolutions shown in the panels.

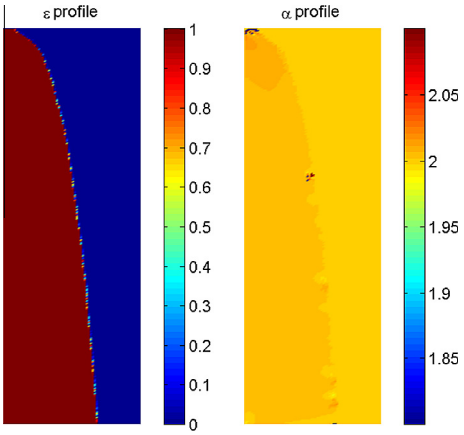

Fig. 10. A snapshot of the fluid fraction ϵ and α-profile of a condensation film flow where $L = 1.5$ mm, $Pr = 0.8$ and $Ja = 2.4$.

the corresponding effects require a three-dimensional extension of the model which is beyond the scope of the present paper.

Finally, a comment on the use of the entropic LB scheme instead of the conventional LBGK is in order. As mentioned earlier, the source of numerical instability in the free surface flows is the surface itself. To prove this a snapshot of the α-profile of a condensation film flow where $L = 1.5$ mm, $Pr = 0.8$ and $Ja = 2.4$ is shown in

Fig. 10. To visualize the film the fluid fraction ϵ is also shown in Fig. 10. This simulation was proven to be unstable with the standard LBGK but it is stable using the ELB model. In Fig. 10 it is seen that the entropic estimations are activated, at this snapshot, mainly in two places at the surface. Furthermore, the α values cover a range of 1.8 to 2.05. We remind that the conventional LBGK corresponds to the fixed value $\alpha = 2$. The need for the entropic stabilization is therefore clear.

4. Conclusion

A free surface entropic lattice Boltzmann approach has been introduced and the model is applied to predict steady laminar film condensation on a flat vertical hydrophilic surface. The model framework enables to reach Prandtl and Jakob numbers not reported before for lattice Boltzmann simulations of film condensation. Furthermore, the model allows film condensation modeling beyond the laminar regime and it shows good agreement with earlier developed empirical models in a relatively wide range of film Reynolds numbers.

The presented model is developed for simulations of saturated vapor. However, adjustment of the mass balance equation at the interface can allow to model condensation of non-uniformly saturated vapor, thus, extending use of the model. Furthermore, evaporation can be introduced in the model as further development of the approach.

Since the model displays good agreement with empirical models for film condensation beyond the laminar flow the next improvement would be to develop accurate simulations of turbulent film flows in three dimensions.

Conflict of interest

None declared.

Acknowledgment

This work is a part of research activities within the Center of Reliable Power Electronics (CORPE) funded by the Danish Strategic Research Council. We thank the Aerothermochemistry and Combustion Systems Laboratory of ETH for the hospitality during the stay of M.A.H. and Shyam Chikatamarla for helping setting up the ELB simulations in the beginning.

I.V.K. gratefully acknowledges support by the ERC Advanced Grant 291094-ELBM.

References

[1] R. Bird, W. Stewart, E. Lightfoot, Transport Phenomena, Wiley, Wiley International edition, 2007.
[2] S. Ghiaasiaan, Two-Phase Flow, Boiling, and Condensation, Cambridge University Press, In Conventional and Miniature Systems, 2007.
[3] W. Nusselt, Die Oberflachenkondesation des Wasserdamffes the surface condensation of water, Zetrschr. Ver. Deutch. Ing. 60 (1916) 541–546.
[4] M.M. Chen, An analytical study of laminar film condensation: part 1flat plates, J. Heat Transfer 83 (1) (1961) 48–54.
[5] J. Koh, E. Sparrow, J. Hartnett, The two phase boundary layer in laminar film condensation, Int. J. Heat Mass Transfer 2 (1) (1961) 69–82.
[6] P.L. Kapitza, Wave flow of thin layers of a viscous fluid, i. the free flow, Zh. Eksperim. Theor. Fiz. 18 (3) (1916) 541–546.
[7] F. Higuera, S. Succi, R. Benzi, Lattice gas dynamics with enhanced collisions, EPL (Europhys. Lett.) 9 (4) (1989) 345–349.
[8] Y. Qian, D. d'Humières, P. Lallemand, Lattice BGK models for Navier-Stokes equation, EPL (Europhys. Lett.) 17 (6) (1992) 479–484.
[9] X. Shan, X. He, Discretization of the velocity space in the solution of the Boltzmann equation, Phys. Rev. Lett. 80 (1998) 65–68.
[10] I.V. Karlin, A.N. Gorban, S. Succi, V. Boffi, Maximum entropy principle for lattice kinetic equations, Phys. Rev. Lett. 81 (1998) 6–9.
[11] I. Karlin, A. Ferrante, H. Öttinger, Perfect entropy functions of the lattice Boltzmann method, EPL (Europhys. Lett.) 47 (2) (1999) 182–188.
[12] S. Ansumali, I. Karlin, H. Öttinger, Minimal entropic kinetic models for hydrodynamics, EPL (Europhy. Lett.) 63 (6) (2003) 798–804.
[13] S. Ansumali, I.V. Karlin, H.C. Öttinger, Thermodynamic theory of incompressible hydrodynamics, Phys. Rev. Lett. 94 (2005) 080602.
[14] S. Ansumali, I.V. Karlin, Consistent lattice Boltzmann method, Phys. Rev. Lett. 95 (2005) 260605.
[15] S. Succi, The Lattice-Boltzmann Equation, Oxford University Press, Oxford, 2001.
[16] X. Liu, P. Cheng, Lattice Boltzmann simulation of steady laminar film condensation on a vertical hydrophilic subcooled flat plate, Int. J. Heat Mass Transfer 62 (2013) 507–514.
[17] X. Liu, P. Cheng, Lattice Boltzmann simulation for dropwise condensation of vapor along vertical hydrophobic flat plates, Int. J. Heat Mass Transfer 64 (2013) 1041–1052.
[18] I. Ginzburg, K. Steiner, Lattice Boltzmann model for free-surface flow and its application to filling process in casting, J. Comput. Phys. 185 (1) (2003) 61–99.
[19] N. Thürey, C. Körner, U. Rüde, Interactive free surface fluids with the lattice Boltzmann method, Technical Report 05-4. University of Erlangen-Nuremberg, Germany.
[20] U. Rüde, N. Thürey, Free surface lattice-Boltzmann fluid simulations with and without level sets, in: Vision, Modeling, and Visualization 2004: Proceedings, November 16–18, 2004, USA, IOS Press, Standford, 2004, p. 199.
[21] N. Thürey, U. Rüde, Stable free surface flows with the lattice Boltzmann method on adaptively coarsened grids, Comput. Visual. Sci. 12 (5) (2009) 247–263.
[22] I.V. Karlin, S. Succi, S.S. Chikatamarla, Comment on numerics of the lattice Boltzmann method: effects of collision models on the lattice boltzmann simulations, Phys. Rev. E 84 (2011) 068701.
[23] A. Kupershtokh, New method of incorporating a body force term into the lattice Boltzmann equation, in: Proceedings of the 5th International EHD Workshop, University of Poitiers, Poitiers, France, 2004, pp. 241–246.
[24] S.S. Chikatamarla, S. Ansumali, I.V. Karlin, Entropic lattice Boltzmann models for hydrodynamics in three dimensions, Phys. Rev. Lett. 97 (2006) 010201.
[25] X. He, S. Chen, G.D. Doolen, A novel thermal model for the lattice boltzmann method in incompressible limit, J. Comput. Phys. 146 (1) (1998) 282–300.
[26] I.V. Karlin, D. Sichau, S.S. Chikatamarla, Consistent two-population lattice Boltzmann model for thermal flows, Phys. Rev. E 88 (2013) 063310.
[27] N. Thürey, C. Wojtan, M. Gross, G. Turk, A multiscale approach to mesh-based surface tension flows, ACM Transactions on Graphics (TOG), Vol. 29, ACM, 2010. p. 48..
[28] X. Xing, D.L. Butler, C. Yang, A lattice boltzmann based single-phase method for modeling surface tension and wetting, Comput. Mater. Sci. 39 (2) (2007) 282–290.
[29] Q. Zou, X. He, On pressure and velocity boundary conditions for the lattice Boltzmann BGK model, Phys. Fluids 9 (6) (1997) 1591–1598 (1994-present).
[30] S. Kutateladze, Semi-empirical theory of film condensation of pure vapours, Int. J. Heat Mass Transfer 25 (5) (1982) 653–660.
[31] S. Chen, F. Gerner, C. Tien, General film condensation correlations, Exp. Heat Transfer Int. J. 1 (2) (1987) 93–107.